

Unconventional Magnon Blockade Under the Sagenac Fizeau Shift in an Opto-Magnonic System: Parametric Amplification



Anjan Samanta, Pinku Jana, Paresh Chandra Jana

Abstract: We propose to achieve and enhance the unconventional magnon blockade effect, based on a quantum destructive interference mechanism in an optomechanical-magnetic system composed of a rotating cavity and a yttrium iron-garnet (YIG) sphere. We introduce a degenerate parametric amplifier and derive the optimal parametric gain and phase to achieve magnon blockade analytically. By tuning the system parameters (weak coupling) and the driving detuning of the cavity and magnon modes, we achieve the smallest second-order magnon correlation function. The optomechanical cavity couples to the YIG sphere by magnetic dipole interaction. We achieve unconventional magnon blockade effects when the cavity is driven from a clockwise or counterclockwise direction. We introduce a new feature that combines the impact of destructive interference and energy-level anharmonicity to achieve magnon blockade. The equal-time second-order magnon correlation avoids time delay and rapid oscillation. In the input end of the system, two photons drive, and complete quantum destructive interference. This study opens a new window for physical applications, including the generation of single magnon sources, Quantum sensing, and Quantum simulation. Experimentally, we can control quantum noise and amplify the signal using parametric amplification.

Key Words: Magnon Blockade, Sagenac-Fizeau shift, parametric amplification,

I. INTRODUCTION

Magnon Blockade is a nonlinear phenomenon observed in different optical and optomechanical systems and is also a topic of research interest. The concept of the blockade effect using a laser diode was first analyzed in 1964 by G. J. Lasher [1]. Earlier blockade research work concentrated on a two-level atomic system, as the nuclear media provide resonantly enhanced nonlinearity. However, due to strong resonant absorption, the applications of a two-level system are restricted. Optical systems may overcome this challenge. In 1983, Dorsel et al first experimentally observed the blockade in the field of optical cavity systems [2].

Manuscript received on 01 June 2025 | First Revised Manuscript received on 08 June 2025 | Second Revised Manuscript received on 12 June 2025 | Manuscript Accepted on 15 June 2025 | Manuscript published on 30 June 2025.

*Correspondence Author(s)

Anjan Samanta*, Department of Physics, Vidyasagar University, Midnapore, (West Bengal), India. Email ID: anjan.samanta744@gmail.com, ORCID ID: [0000-0001-8037-3066](https://orcid.org/0000-0001-8037-3066)

Pinku Jana, Department of Physics, Vidyasagar University, Midnapore, West Bengal, India. Email ID: pinku@sabangcollege.ac.in, ORCID ID: [0009-0000-4235-8519](https://orcid.org/0009-0000-4235-8519)

Paresh Chandra Jana, Department of Physics, Vidyasagar University, Midnapore, (West Bengal), India. Email ID: pareshjana@rediffmail.com, ORCID ID: [0000-0002-4868-0223](https://orcid.org/0000-0002-4868-0223)

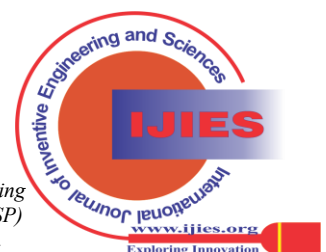
© The Authors. Published by Blue Eyes Intelligence Engineering and Sciences Publication (BEIESP). This is an open access article under the CC-BY-NC-ND license <http://creativecommons.org/licenses/by-nc-nd/4.0/>

Recently, the blockade of mean cavity photon number in various systems has been extensively studied, including semiconductor ring lasers, two-mode optomechanics, ring cavity double quantum dot molecules, Kerr nonlinear gaseous media, optomechanical systems with two-level atoms, photonic crystal nanocavities, hybrid optomechanical systems, and photonic-molecule optomechanics, among others [3]. The blockade nature is not only confined to the field of photonic systems, but it has also already been reported in the field of mechanical cavity-polariton magnetic, and cavity-transmon systems, and these are termed phononic blockade, polaritonic blockade, magnon blockade, and transmon blockade, respectively [4].

Different types of nonlinear media offer blockade in various systems, such as the Kerr medium, semiconductor microcavity, and superconducting qubit, among others [5]. There are numerous works regarding bistability with Kerr media, for example, self-Kerr atomic gaseous media in a ring cavity, two-cavity magnonics systems, and coupled cavity systems [6]. Again, the First experimental evidence of blockade in semiconductor microcavities under strong coupling was performed by A. Bass et al [7]. Other experimental works were conducted by N. A. Gippius et al. and Ye-Larionova et al. regarding blockade in a semiconductor microcavity system. Y. Zhang et al theoretically investigated blockade in semiconductor microcavities in the presence of two lasers driving two cavity modes [8], [9]. These studies are all fascinating and impactful. However, all these studies are confined to fixed microcavity setups. However, to the best of our knowledge, rotation-based blockade has not been explored yet [10]. In the present work, we consider a rotating cavity system composed of III-V non-centrosymmetric semiconductor material and study the possibility of magnon blockade [11], [12]. We have proposed single-laser driving, where the cavity is driven from both its left and right sides [13], [14]. Rotating cavity resonator systems are essential in nanoparticle sensing and slow light generation [15].

Magnon Blockade shall have practical applications in designing more efficient logic gate devices, optical switches, ultra-compact optical storage, all-optical wavelength converters, power limiters, optical transistors, memory elements, sensitive force detections, signal processing for quantum computing and solid-state quantum information processing [16][32]. Motivated by potential utility, we have illustrated the Blockade mechanism in this article.

In this report, we theoretically analyse the Magnon Blockade phenomena in a rotating semiconductor micro-cavity system. This brief report is arranged as follows:



Published By:
 Blue Eyes Intelligence Engineering
 and Sciences Publication (BEIESP)
 © Copyright: All rights reserved.

first, we describe the theoretical model and stationary solution of the field mode by using the Heisenberg-Langevin equation of motion analytically and also numerically. Then we discussed the obtained results. At last, a conclusion is presented.

II. THE MODEL

Consider a cavity-magnon system presented in Figure 1. The optical cavity consists of a second-order nonlinearity and an optogenetic cavity [17]. The model Hamiltonian is given by [18], [19]:

$$H = H_o + H_I + H_d \dots (1)$$

where $H_o = \omega_a a^\dagger a + \omega_b b^\dagger b + \omega_m m^\dagger m$, describes the free evolution of the cavity system with bosonic annihilation operators a and b . a Mode corresponds to the fundamental mode with frequency. ω_a and b for the second harmonic mode with frequency ω_b , respectively and $m^\dagger(m)$ Is the creation (annihilation) operator of the magnon mode, where ω_m Is the eigenfrequency of the magnon mode [20]. The typical value of the cavity resonance frequency of the fundamental mode $\omega_a = 2\pi \times 163.195$ THz and the quality factors for a and b modes are $Q_a = 1.6 \times 10^4$ and $Q_b = 3.2 \times 10^4$, respectively (if decay rates of both modes are the same), as reported in a micro-ring system [21], [22]. The part of the Hamiltonian H_I Denotes the interaction when two optical fields meet, which can be written as $H_I = g(ba^{\dagger 2} + b^\dagger a^2) + g_{ma}(am^\dagger + a^\dagger m)$, where g is the photon hopping strength and g_{ma} denotes the coupling coefficient between the magnon and photon mode [23]. The strength related to nonlinear terms via the relation

$$g = \sqrt{\frac{\hbar\omega_a}{2\epsilon_0 n_a^2 V_a} \frac{\omega_b}{2n_b^2 V_b}} \int dv \chi_{ijk}^{(2)}(r) E_a^i(r) E_b^j(r) E_b^k(r) \dots (2)$$

Where $V_{a,b}$ Indicate the mode volume, $\chi_{ijk}^{(2)}(r)$ is the nonlinear susceptibility tensor, $E_{a,b}(r)$ represent the spatial part of the field mode and follow the normalization condition

$\int dr |E_{a,b}(r)|^2 = 1$ and $n_{a,b}$ Denote the number of photons for the optical field modes [24]. Second-order nonlinearity provides the conversion of a photon of mode a to two photons of the mode b or vice-versa. The cavity with $\chi^{(2)}$ Nonlinear materials are made of III-V semiconductors, which are non-centrosymmetric [25]. The materials are higher $\chi^{(2)}$ such as GaAs, AlGaAs, GaN, BN, AlN and AlGaIn [26], [37]. The photon hopping strength depends on the III-V semiconductor material used in the cavity [27], [28]. The typical value of hopping strength is $\hbar g \approx 2 \times 10^{-5}$ eV as reported in experimental demonstration [29], [38]. The last part of the Hamiltonian H_d describes the external driving field and reads as $H_d = \Omega(a^\dagger e^{-i\omega_{L1}t} - a e^{i\omega_{L1}t}) + F(m^\dagger e^{-i\omega_{L2}t} - m e^{i\omega_{L2}t})$, where ω_{L1} and Ω are the driving frequency and the driving amplitude, respectively, and those of the magnon mode are ω_{L2} and F with $\omega_{L1} = \omega_{L2} = \omega_L$. The input power P relates to the driving amplitude by $\Omega = \sqrt{2k_a P / \hbar \omega_L}$, where k_a denotes the decay rate of the mode a .

For a cavity resonator rotating at a fixed angular speed ω_r , the light circulating in the cavity resonator experiences a Sagnac-Fizeau shift, and the cavity resonance frequency is modified by $\omega_k \rightarrow \omega_k + \Delta_{SFk}$ [30]. The amount of shift is given by

$$\Delta_{SFk} = \pm \frac{nr\omega_k\omega_r}{c} \left(1 - \frac{1}{n^2} - \frac{\lambda}{n} \frac{dn}{d\lambda}\right) \dots (3)$$

Where $k = a, b, m$; n is the refractive index, r Is the radius of the cavity, λ and c are the wavelength and speed of light in free space [31], [32]. The angular acceleration of the cavity's rotation may vary from a few Hz to several GHz, as demonstrated in various experimental studies and theoretical investigations [33]. The Sagnac-Fizeau shift directly depends on the rotational speed of the cavity and the direction of input driving fields [34]. $\Delta_{SFk} < 0$ and $\Delta_{SFk} > 0$ Indicates that the external input light propagates along and against the direction of rotation of the cavity, i.e., the cavity is driven from its right and left, respectively, as shown in Figure 1b.

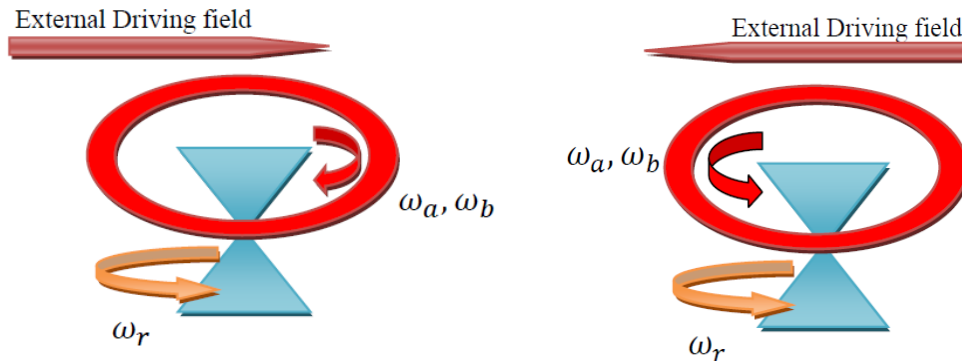


[Fig.1: Schematic Depiction of Rotating Cavity System. When an External Field drives the Cavity from its (i) Left Side and (ii) Right Side]

Considering the shift, the Hamiltonian becomes

$$H_s = (\omega_a + \Delta_{SFa})a^\dagger a + (\omega_b + \Delta_{SFb})b^\dagger b + \omega_m m^\dagger m + g(ba^{\dagger 2} + b^\dagger a^2) + g_{ma}(am^\dagger + a^\dagger m) + \Omega(a^\dagger e^{-i\omega_{L1}t} - a e^{i\omega_{L1}t}) + F(m^\dagger e^{-i\omega_{L2}t} - m e^{i\omega_{L2}t}) \dots (4)$$

In the rotating frame of the external driving field, based on the unitary operator $U = e^{\frac{i\omega_L t}{2}}(a^\dagger a + b^\dagger b + m^\dagger m)$, the Hamiltonian of equation (4) takes the form

$$H_r = (\Delta + \Delta_{SF})a^\dagger a + 2(\Delta + \Delta_{SF})b^\dagger b + \Delta_m m^\dagger m + g(ba^{\dagger 2} + b^\dagger a^2) + g_{ma}(am^\dagger + a^\dagger m) + \Omega(a^\dagger - a) + F(m^\dagger - m) \dots \quad (5)$$

with $\Delta = \omega_a - \omega_L$, $\Delta_m = \omega_m - \omega_L$. According to the second harmonic generation $\omega_b = 2\omega_a$, if we consider $\Delta_{SF_a} = \Delta_{SF}$ then $\Delta_{SF_b} = 2\Delta_{SF}$.

The eigenvalue equation of the system Hamiltonian can be expressed as $H|\Psi_j\rangle = E_j|\Psi_j\rangle$, where $j = 0, 1, 2, \dots$. E_j are the eigenenergies of the non-rotating system [35]. The eigenstates are $|\Psi_j\rangle$ and can be expressed in terms of a Fock state $|n_a, n_b, n_m\rangle$, n_a, n_b are the number of photons in a and b modes and n_m be the number of magnons in m mode, respectively. Due to the rotation of the cavity, the eigenenergies are modified by the term $\pm j\hbar|\Delta_{SF}|$, where \pm corresponds to the upper and lower shifting of energy. E_j , respectively [44]. The rotational speed of the cavity would follow the condition, $|\Delta_{SF}| = g/2\sqrt{2}$ [45], [49]. We assume that the condition. $2\omega_m \approx \omega_L \ll \omega_a$ is satisfied, indicating that the cavity and magnon mode, owing to the larger frequency difference [36]. To achieve a reliable numerical calculation, we introduce the master equation for the density matrix. ρ of the cavity magnon mode system.

$$\frac{d\rho}{dt} = -i[H_r, \rho] + \sum_k \gamma_k (L_k \rho L_k^\dagger - \frac{1}{2}\{L_k^\dagger L_k, \rho\}) \dots \quad (6)$$

Where $\gamma_k (k = a, b, m)$ are the decay rates, and L_k The Lindblad (dissipation) Operator represents the system-environment interactions. For cavity damping $L_a = \sqrt{\gamma_a} a$, γ_a photon loss rates, for mechanical damping $L_b = \sqrt{\gamma_b} b$, γ_b phonon loss rates, for the magnon mode $L_m = \sqrt{\gamma_m} m$, γ_m Magnon loss rates [37], [38].

To obtain the statistical properties of the magnon mode, we introduce the equal-time second-order correlation function in the form:

$$g_{mm}^2(0) = \frac{Tr(m^{\dagger 2} m^2 \rho_{ss})}{[Tr(m^\dagger m \rho_{ss})]^2} = \frac{\langle m^{\dagger 2} m^2 \rangle}{\langle m^\dagger m \rangle^2} \dots \quad (7)$$

Where ρ_{ss} is the steady-state solution of the master equation. The second-order correlation function $g_{mm}^2(0)$ could represent the single magnon degree. Where $g_{mm}^2(0) < 1$ indicates the sub-Poissonian statistics and magnon blockade and $g_{mm}^2(0) > 1$ Corresponds to super-Poissonian statistics.

In the next section, we plot the mean magnon number and the behaviour of $g_{mm}^2(0)$ as a function of system parameters, and give the energy level transition paths.

III. UNCONVENTIONAL MAGNON BLOCKADE

Here, we investigate the unconventional magnon blockade for this system. Now, the non-classical effects can be utilised by simplifying the energy level transition of this system. Under the weak coupling ($g, g_{ma} \ll \Delta, \Delta_m, \Delta_m$) and driving conditions ($F, \Omega \ll \Delta, \Delta_m, \Delta_m$) The Hamiltonian simplifies, and we analyse the energy level transitions using perturbation

theory and the dressed-state picture, which can modify the transition frequency [39]. For the cavity mode, the allowed transitions are: $|n_a, n_b, n_m\rangle \rightarrow |n_a \pm 1, n_b, n_m\rangle$ due to $\Omega(a^\dagger - a)$, the detuning $\Delta + \Delta_{SF}$ Shifts the effective resonance frequency. For the magnon mode transitions $|n_a, n_b, n_m\rangle \rightarrow |n_a, n_b, n_m \pm 1\rangle$ due to $F(m^\dagger - m)$, the weak coupling g_{ma} Induces hybridization between magnon and photon states [40]. The steady-state wavefunction $|\psi\rangle$ of the system can be written as a linear combination of the probability amplitudes C_{am} and the corresponding basis states $|am\rangle$. Under the weak coupling regimes, the wave function of the optomechanical system can be expanded (For a truncated Hilbert space with up to N excitations in each mode) approximately: $|\psi\rangle = C_{00}|0,0\rangle + C_{01}|0,1\rangle + C_{10}|1,0\rangle + C_{11}|1,1\rangle + C_{20}|2,0\rangle + C_{02}|0,2\rangle + \dots$

So the Schrodinger equation of the system Hamiltonian is:

$$|\psi(t)\rangle = \sum_{a,m} C_{am}(t)|a, m\rangle \dots \quad (8)$$

Substituting into the Schrodinger equation

$$i\hbar \sum_{a,m} \frac{d}{dt} C_{am}(t)|a, m\rangle = H \sum_{a,m} C_{am}(t)|a, m\rangle$$

$$i\hbar \frac{d}{dt} C_{am} = (\Delta + \Delta_{SF})a C_{am} + 2(\Delta + \Delta_{SF})m C_{am} + \Delta_m m C_{am} + g[\sqrt{(a+1)(a+2)}C_{(a+2)m} + \sqrt{a(a-1)}C_{(a-2)m}] + g_{ma}[\sqrt{(a+1)}C_{(a+1)(m-1)} + \sqrt{m}C_{(a-1)(m+1)}] + \Omega[\sqrt{(a+1)}C_{(a+1)m} - \sqrt{a}C_{(a-1)m}] + F[\sqrt{(m+1)}C_{a(m+1)} - \sqrt{m}C_{a(m-1)}] \dots \quad (9)$$

The set of coupled differential equations is

Vacuum State $|0,0\rangle : i \frac{d}{dt} C_{00} = \Omega C_{10} + F C_{01}$

One Magnon State $|0,1\rangle : i \frac{d}{dt} C_{01} = (\Delta_m + 2(\Delta + \Delta_{SF}))C_{01} + F C_{00} + g_{ma} C_{10}$

One Photon State $|1,0\rangle : i \frac{d}{dt} C_{10} = (\Delta + \Delta_{SF})C_{10} + \Omega C_{00} + g_{ma} C_{01}$

Two-Photon State $|2,0\rangle : i \frac{d}{dt} C_{20} = 2(\Delta + \Delta_{SF})C_{20} + \sqrt{2}\Omega C_{10} + g C_{02}$

Two-Magnon State $|0,2\rangle : i \frac{d}{dt} C_{02} = 2(\Delta_m + 2(\Delta + \Delta_{SF}))C_{02} + \sqrt{2}F C_{01} + g_{ma} C_{20}$

One Photon one Magnon State $|1,1\rangle : i \frac{d}{dt} C_{11} = (\Delta + \Delta_{SF} + \Delta_m)C_{11} + F C_{10} + \Omega C_{01} + g_{ma} C_{20} + g_{ma} C_{02}$

For the steady-state solution, we set the time derivatives of all probability amplitudes. $C_{am} = 0$. So, from the previously derived coupled differential equations, we get:

$$0 = \Omega C_{10} + F C_{01}$$

$$0 = (\Delta_m + 2(\Delta + \Delta_{SF}))C_{01} + F C_{00} + g_{ma} C_{10}$$

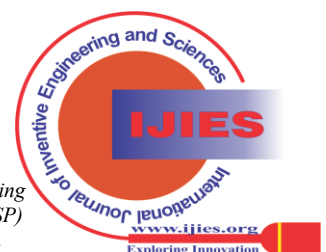
$$0 = (\Delta + \Delta_{SF})C_{10} + \Omega C_{00} + g_{ma} C_{01}$$

$$0 = 2(\Delta + \Delta_{SF})C_{20} + \sqrt{2}\Omega C_{10} + g C_{02}$$

$$0 = 2(\Delta_m + 2(\Delta + \Delta_{SF}))C_{02} + \sqrt{2}F C_{01} + g_{ma} C_{20}$$

$$0 = (\Delta + \Delta_{SF} + \Delta_m)C_{11} + F C_{10} + \Omega C_{01} + g_{ma} C_{20} + g_{ma} C_{02}$$

We solve these equations in a matrix inversion method, so the matrix form of this equation is (Appendix [A]):



Unconventional Magnon Blockade Under the Sagnac Fizeau Shift in an Opto-Magnonic System: Parametric Amplification

$$\begin{pmatrix} 0 & 0 & \Omega & 0 & 0 & F \\ 0 & (\Delta_m + 2(\Delta + \Delta_{SF})) & g_{ma} & 0 & 0 & F \\ \Omega & g_{ma} & (\Delta + \Delta_{SF}) & 0 & 0 & 0 \\ 0 & 0 & \sqrt{2}\Omega & 2(\Delta + \Delta_{SF}) & g & 0 \\ 0 & \sqrt{2}F & 0 & g_{ma} & 2(\Delta_m + 2(\Delta + \Delta_{SF})) & 0 \\ 0 & \Omega & F & g_{ma} & g_{ma} & (\Delta + \Delta_{SF} + \Delta_m) \end{pmatrix} \begin{pmatrix} C_{00} \\ C_{01} \\ C_{10} \\ C_{20} \\ C_{02} \\ C_{11} \end{pmatrix} = \begin{pmatrix} 0 \\ 0 \\ 0 \\ 0 \\ 0 \\ 0 \end{pmatrix}$$

Now we compute the second-order correlation function, $g_{mm}^2(0)$, with the help of the steady-state probability amplitudes. Now, the expectation values using the probability amplitudes are the mean number of magnons.

$$\begin{aligned} \langle m^\dagger m \rangle &= 1|C_{10}|^2 + 2|C_{20}|^2 + 1|C_{11}|^2 \\ \langle m^{\dagger 2} m^2 \rangle &= 2|C_{20}|^2 \end{aligned}$$

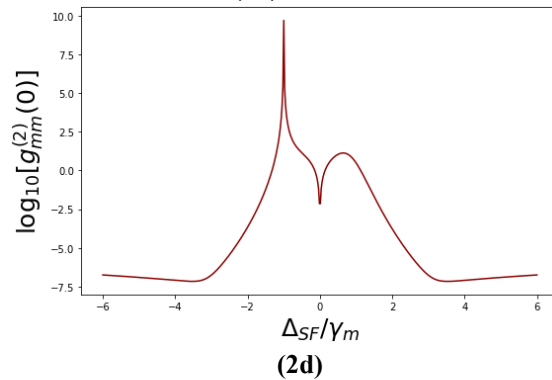
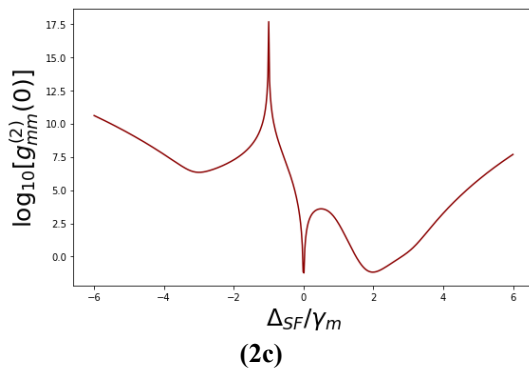
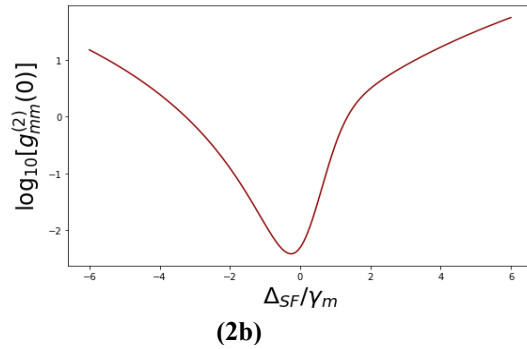
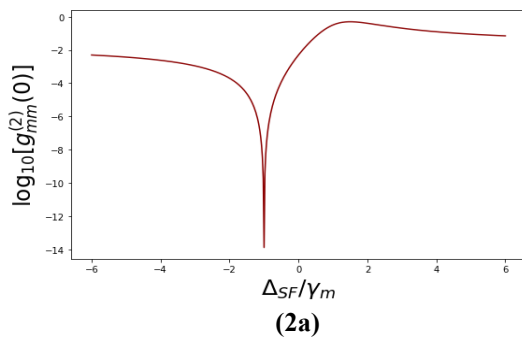
$$\text{So the second-order correlation } g_{mm}^2(0) = \frac{2|C_{20}|^2}{(1|C_{10}|^2 + 2|C_{20}|^2 + 1|C_{11}|^2)^2} \dots (10)$$

IV. RESULTS AND DISCUSSIONS

In this section, we present the magnon antibunching effect using both numerical and analytical simulations under a rotational opto-magnonic system. The Sagnac-Fizeau shift directly depends on the rotational speed of the cavity and also on the direction of the input driving fields. $\Delta_{SF_k} < 0$ and $\Delta_{SF_k} > 0$ indicates that the external input light propagates along and against the direction of rotation of the cavity, i.e., the cavity is driven from its right and left [41]. Here, we investigate the unconventional magnon blockade under the Sagnac Fizeau shift in an opto-magnonic system. Non-classical phenomena can be analysed both analytically and numerically under weak coupling and driving mechanisms. Surprisingly, we achieved the antibunching condition, and destructive interference occurs between the transition paths, so we conclude that unconventional magnon blockade was perfectly achieved. Our analytical results agree with the

numerical results but differ slightly in the optimal situation. This is due to perturbation in analytical simulation, where quantum jumps are neglected in finite dimensions. In contrast, numerical simulation utilises the Lindblad master equation, allowing the magnon and photon to remain in the same state under minimal driving conditions.

We numerically solve the system to compute $g_{mm}^2(0)$ for the magnon mode to study the statistical property of the magnon mode using the QuTiP package in Python. In Figures 2a- 2h, we first investigate analytically the effect of the second-order correlation function, $(\log_{10}(g_{mm}^2(0)))$ as a function of normalized Sagnac Fizeau shift and normalized by magnon loss rates (γ_m) [42]. The system is driven in both clockwise and counterclockwise directions. We observe from Figure 2 that when the cavity is driven in the clockwise and counterclockwise directions, the second-order correlation function is less than or greater than one, indicating the magnon antibunching and bunching effects. The statistical property of the magnon satisfies a sub-Poissonian distribution and super-Poissonian situation under the above condition, so that a single magnon can be achieved due to the opposite Sagnac Fizeau shift [43]. We achieved that when the $\Delta_m = 0$, the value of $\log_{10}(g_{mm}^2(0)) \sim -14$ and $\log_{10}(g_{mm}^2(0)) \sim 17.5$ (Fig. -2h) under the various system parameters, which implies the unconventional magnon blockade under the Sagnac Fizeau shift



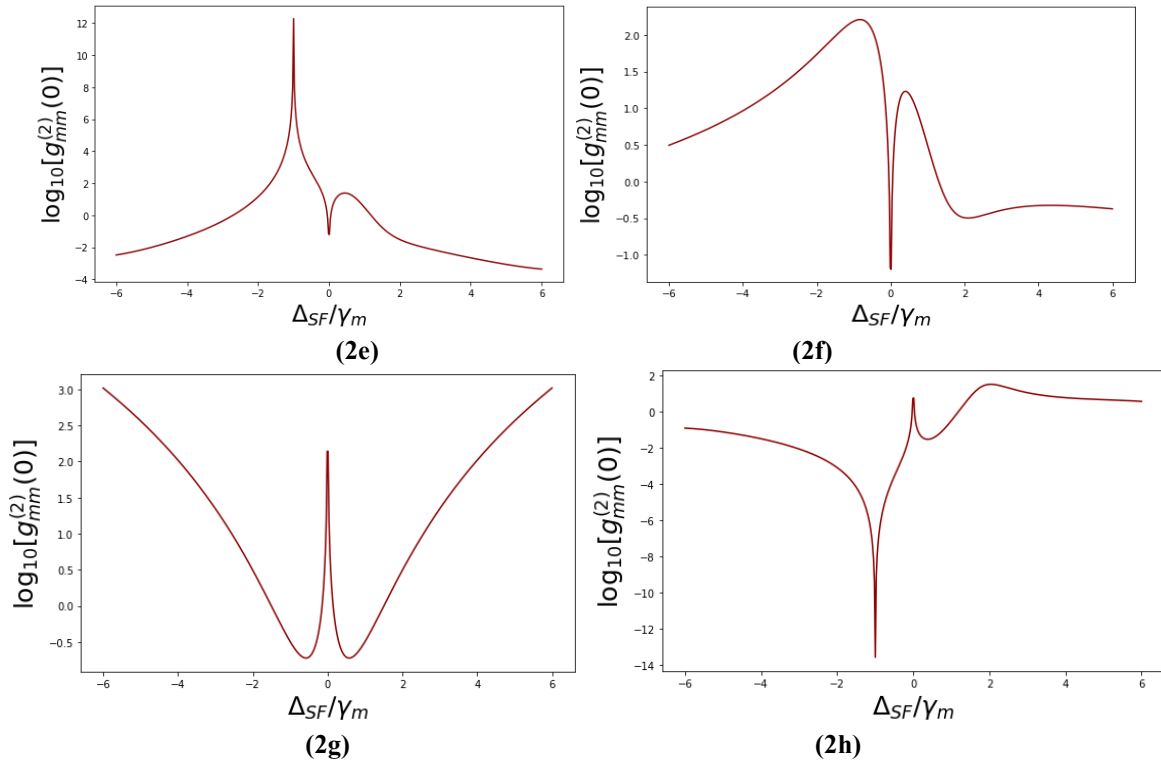
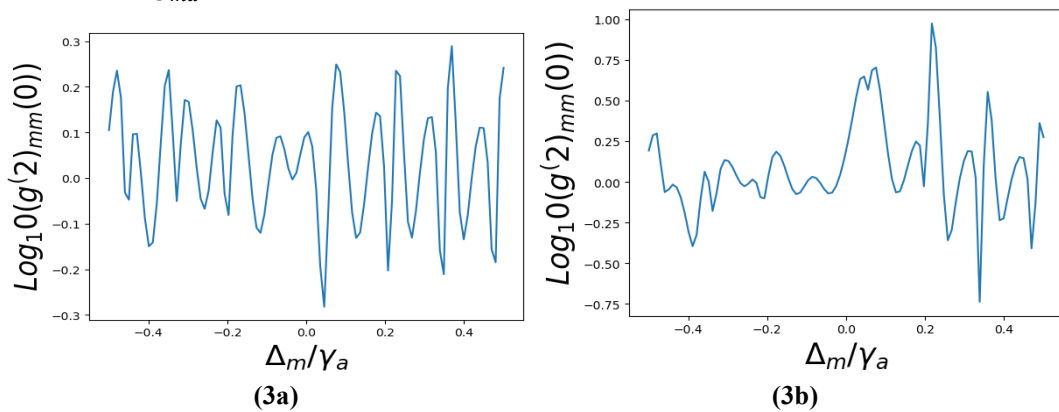


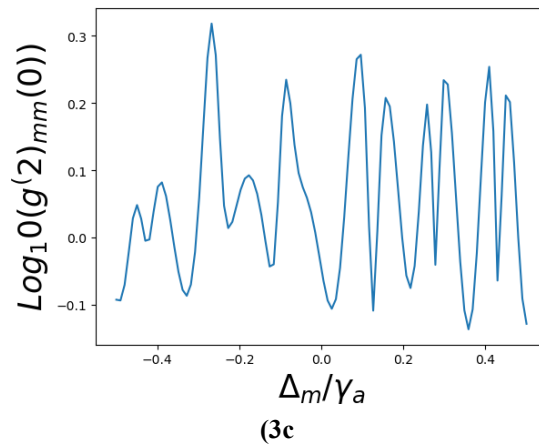
[Fig.2: Second-Order Correlation Function as a Function of Sagenac Fizeau Shift Normalized by Magnon Decay Rates. (2a-2c): $g_{ma} = 2\pi \times 1.0$ MHz, $F = 0.01$ N/m, $\gamma_m = 0.2$ GHz, $\Omega = 2\pi \times 1$ GHz, (2a) $\Delta/\gamma_m = 1.0$, $\Delta_{SF}/\gamma_m = 8.5$, $g = 2\pi \times 0.1$ MHz, 1.0 , $\Delta_m/\gamma_m = 1.0$, (2b) $\Delta/\gamma_m = 1.5$, $\Delta_{SF}/\gamma_m = 8.5$, $g = 2\pi \times 0.5$ MHz, 1.0 , $\Delta_m/\gamma_m = 1.5$, (2c) $\Delta/\gamma_m = 1.5$, $\Delta_{SF}/\gamma_m = 8.5$, $g = 2\pi \times 1.5$ MHz, 1.0 , $\Delta_m/\gamma_m = 2.0$, (5d-5f): $g_{ma} = 0$, $F = 0.05$ N/m, $\gamma_m = 0.2$ GHz, $\Omega = 2\pi \times 1$ GHz, (2d) $\Delta/\gamma_m = 1.0$, $\Delta_{SF}/\gamma_m = 8.5$, $g = 2\pi \times 0.1$ MHz, 1.0 , $\Delta_m/\gamma_m = 1.0$, (2e) $\Delta/\gamma_m = 1.5$, $\Delta_{SF}/\gamma_m = 8.5$, $g = 2\pi \times 0.5$ MHz, 1.0 , $\Delta_m/\gamma_m = 1.5$, (2f) $\Delta/\gamma_m = 1.5$, $\Delta_{SF}/\gamma_m = 8.5$, $g = 2\pi \times 1.5$ MHz, 1.0 , $\Delta_m/\gamma_m = 2.0$]

In Figures 3a- 3c, we plot $\log_{10}(g^2_{mm}(0))$ as a function of normalized Δ_m numerically and normalized by cavity decay rates γ_a . In this section, the magnon blockade emerges from nonlinear interaction and the presence of strong coupling. The strong photon-magnon coupling g_{ma} Hybridises photons and magnons, which enables the magnon blockade. In our system, the practical Kerr nonlinear terms exceed dissipation, allowing magnon blockade to manifest as the suppression of multi-magnon excitations. To achieve the magnon blockade numerically, we neglected the fast-oscillating terms and then simplified the numerical calculations. The other system parameters are: $\Delta/\gamma_m = 0.5$, $\Delta_{SF}/\gamma_m = 0.05$, $\Delta_m/\gamma_m = 0.55$, $g = 2\pi \times 0.6$ MHz, $g_{ma} = 2\pi \times 0.2$ MHz, $\Omega = 2\pi \times$

0.02 GHz, $F = 0.02$ N/m. To achieve the magnon blockade numerically, we first rotate from the left side and then from the right side, $\Delta_{SF} > 0$ (left side) represents Figure 3a, $\Delta_{SF} < 0$ (right side) represents Figure 3b. Therefore, the sign in the rotating frame affects both the energy spectrum and the nonlinear term. For $\Delta_{SF} > 0$. The energy spectrum favours up-conversion processes that are photon absorption and g enhance energy costs for two-magnon excitations, under which we observed strong anti-bunching effects [44]. $\Delta_{SF} < 0$ The energy spectrum favours a down-conversion process of photon emission that is slightly different but still achieves blockade.



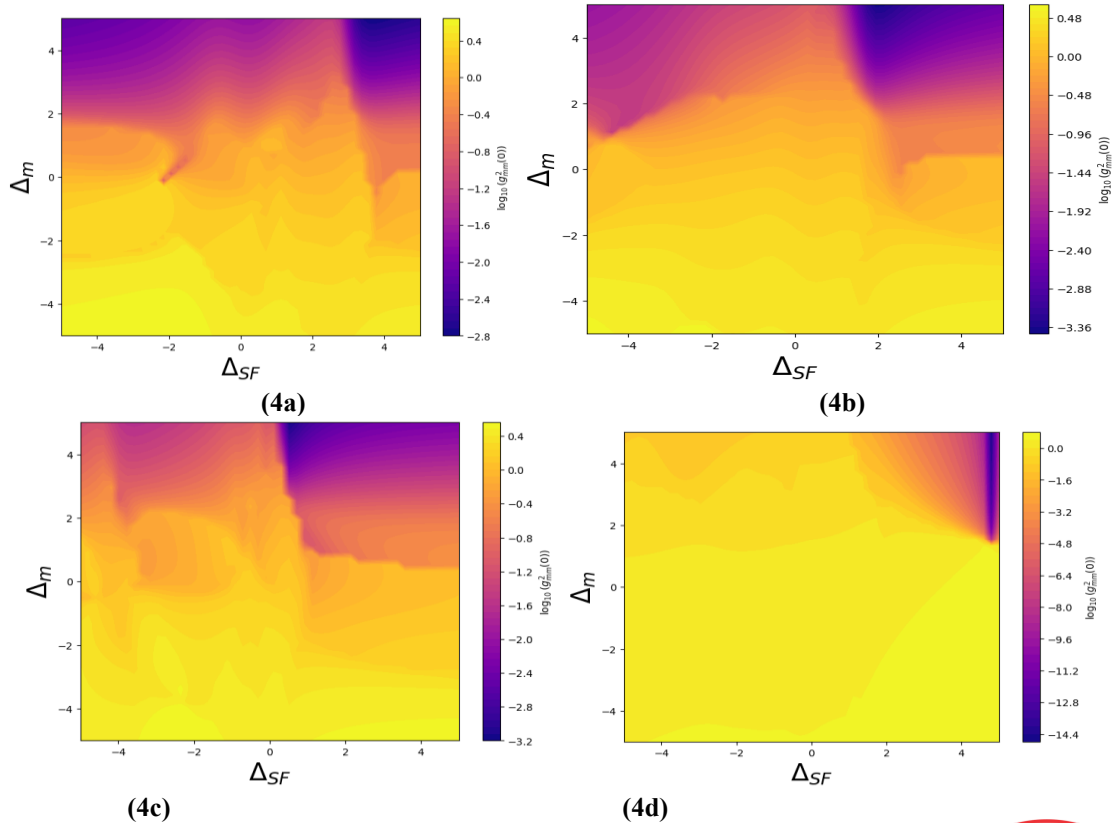
Unconventional Magnon Blockade Under the Sagenac Fizeau Shift in an Opto-Magnonic System: Parametric Amplification



[Fig.3: Second-Order Correlation Function as a Function of Magnon Detuning, Normalised by Cavity Decay Rates, Under a logarithmic scale.(3a-3c): $gma=2\pi\times 1.0$ MHz, $F=0.01$ N/m, $\gamma m=0.2$ GHz, $\Omega=2\pi\times 1$ GHz, (3a) $\Delta/\gamma m=0.5$, $\Delta SF/\gamma m=8.5$, $g=2\pi\times 0.1$ MHz, 1.0, $\Delta m/\gamma m=1.0$, (3b) $\Delta\gamma m=-0.5$, $\Delta SF/\gamma m=-8.5$, $g=2\pi\times 0.5$ MHz, 1.0, $\Delta m/\gamma m=1.5$, (3c) $\Delta/\gamma m=1.5$, $\Delta SF/\gamma m=8.5$, $g=2\pi\times 1.5$ MHz, 1.0, $\Delta m/\gamma m=2.0$]

In Figures 4a- 4f, we plot $\log_{10}(g_{mm}^2(0))$ as a function of Δ_m and Δ_{SF} . Under various system parameters, Figure 4g-4i represents the plot of $\log_{10}(g_{mm}^2(0))$ as a function of Δ_m normalized by γ_m and Δ_a normalized by γ_a . In our study, a rotating cavity containing a magnetic material interacts with microwave photons. When the cavity rotates from left to right (clockwise), the rotational Doppler shift modifies the effective magnon frequency, leading to changes in magnon-photon coupling dynamics. The contour plots of second-order correlation provide information on the blockade mechanism and enhance visualisation. As the cavity rotates left to right, the frequency of the magnon mode modifies at the resonance

condition (Fig. 4g, 4i) and gives $g_{mm}^2(0) < 1$ along the detuning axis, reflecting the change in magnon frequency due to rotation [45]. In Figures 4a, 4b, and 4g, we get a blockade under zero detuning and no rotation. When the cavity rotates left to right, the blockade region shifts right proportional to the rotating rates Figure 4c, 4d. When the cavity rotates right to left, the single line splits into two fragments proportional to the rotating rates, Figure 4h, 4i and indicates double magnon excitation. Therefore, the tunable blockade region with cavity rotation can be leveraged for on-demand control of magnon blockade, which has potential applications in quantum information processing and the study of non-classical states of magnons.



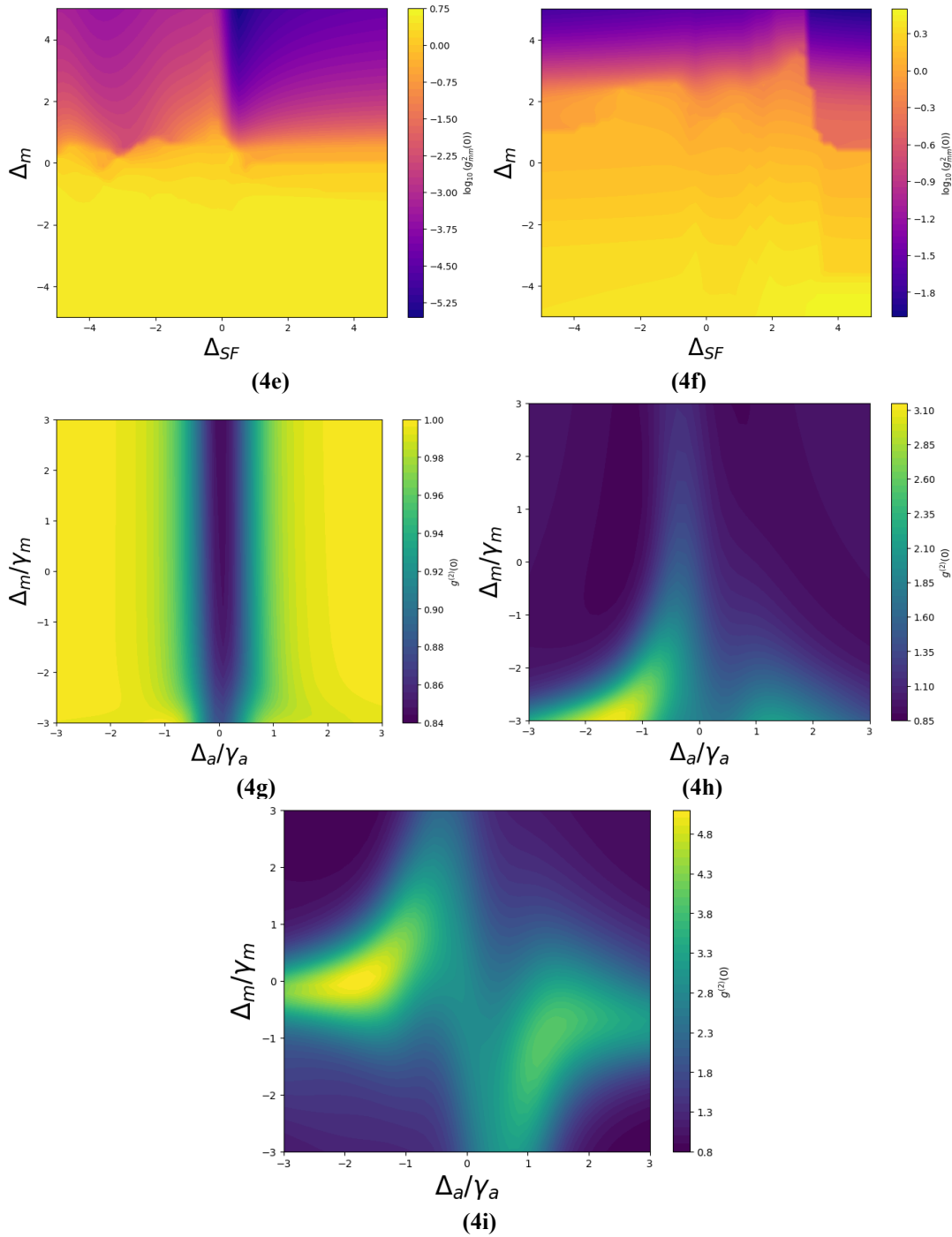


[Fig.4: Second-Order Correlation Function as a Function of Magnon Detuning Under a Logarithmic Scale, as a Function of Magnon Detuning Over Sagenac Fizeau Shift and Magnon Detuning Over Cavity Detuning. (4a-5c): $g_{ma}=2\pi\times 1.0$ MHz, $F=0.01$ N/m, $\gamma_m=0.2$ GHz, $\Omega=2\pi\times 1$ GHz, (5a) $\Delta/\gamma_m=1.0$, $\Delta_{SF}/\gamma_m=8.5$, $g=2\pi\times 0.1$ MHz, 1.0, $\Delta m/\gamma_m=1.0$, (5b) $\Delta/\gamma_m=1.5$, $\Delta_{SF}/\gamma_m=8.5$, $g=2\pi\times 0.5$ MHz, 1.0, $\Delta m/\gamma_m=1.5$, (5c) $\Delta/\gamma_m=1.5$, $\Delta_{SF}/\gamma_m=8.5$, $g=2\pi\times 1.5$ MHz, 1.0, $\Delta m/\gamma_m=2.0$, (5d-5f): $g_{ma}=0$, $F=0.05$ N/m, $\gamma_m=0.2$ GHz, $\Omega=2\pi\times 1$ GHz, (5d) $\Delta/\gamma_m=1.0$, $\Delta_{SF}/\gamma_m=8.5$, $g=2\pi\times 0.1$ MHz, 1.0, $\Delta m/\gamma_m=1.0$, (5e) $\Delta/\gamma_m=1.5$, $\Delta_{SF}/\gamma_m=8.5$, $g=2\pi\times 0.5$ MHz, 1.0, $\Delta m/\gamma_m=1.5$, (5f) $\Delta/\gamma_m=1.5$, $\Delta_{SF}/\gamma_m=8.5$, $g=2\pi\times 1.5$ MHz, 1.0, $\Delta m/\gamma_m=2.0$]

In our Hamiltonian system, the interaction term i Heritia $g_{ma}(am^\dagger + a^\dagger)$ represents the reciprocal coupling, and the interaction non-Hermitian $g_{ma}(am^\dagger)$ represents nonreciprocal coupling. In Figures 5a- 5f, we plot. $\log_{10}(g_{mm}^2(0))$ as a function of temperature for the study of reciprocal and non-reciprocal coupling. In this section, we study the reciprocal and nonreciprocal unconventional magnon blockade effect under the influence of the environmental temperature (T) using the master

equation(equation 6), adding the dissipative term $n_{th}\gamma_m\{L_m[\rho] + L_m^\dagger[\rho]\}$ where the $n_{th} = \frac{1}{e^{\frac{\omega_m}{k_B T}} - 1}$ is the thermal magnon number and k_B be the Boltzmann constant and T be the temperature [46]. We observe the unconventional magnon blockade under various temperature regimes (at high and low-temperature limits). Reciprocal coupling enhances energy sharing ($g_{ma} \neq 0$)

Unconventional Magnon Blockade Under the Sagnac Fizeau Shift in an Opto-Magnonic System: Parametric Amplification

and Non-reciprocal coupling ($g_{ma} = 0$) no energy exchange with the magnon state, so that only the magnon state is thermalised by the driving term F . Figures 5a- 5c represent the high temperature limits $T = 64 \text{ mK}$, $\Delta/\gamma_m = 1.0$, $\Delta_{SF}/\gamma_m = 8.5$, $F = 0.01 \text{ N/m}$, $\Omega = 2\pi \times 1 \text{ At GHz}$, we observe that thermal noise dominates, referred to as thermal bunching, and low temperatures limit this effect. $T = 10 \text{ mK}$, $\Delta/\gamma_m = 2.0$, $\Delta_{SF}/\gamma_m = 8.5$, $F = 0.1 \text{ N/m}$, $\Omega = 2\pi \times 1.5 \text{ At GHz}$,

the magnon starts to be excited from the vacuum, which represents the quantum antibunching effect (figure 5d-5f) [47]. We observed that at the input end of the system, when two photons drive it, complete quantum destructive interference appears and disappears in different paths for two magnon excitations due to the opposite Sagnac Fizeau shifts induced by Fizeau drag, which represents the nonreciprocal unconventional magnon blockade.

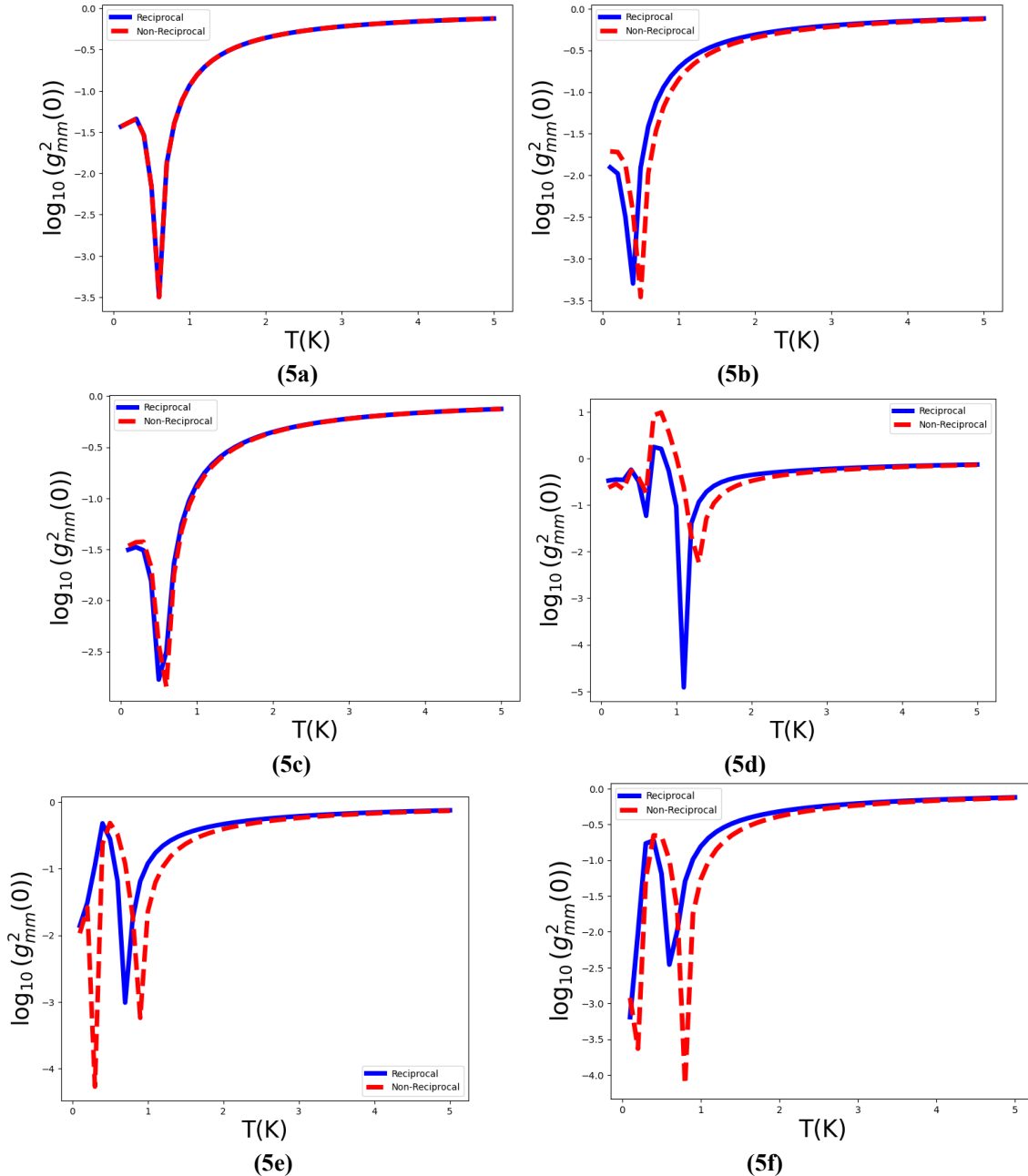


[Fig.5: Second-Order Correlation Function as a Function of Environment Temperature, Magnon Mode, for Different Coupling Modes.(5a-5c): $g_{ma}=2\pi \times 1.0 \text{ MHz}$, $F=0.01 \text{ N/m}$, $\gamma_m=0.2 \text{ GHz}$, $\Omega=2\pi \times 1 \text{ GHz}$, (5a) $\Delta/\gamma_m=1.0$, $\Delta_{SF}/\gamma_m=8.5$, $g=2\pi \times 0.1 \text{ MHz}$, 1.0 , $\Delta m/\gamma_m=1.0$, (5b) $\Delta/\gamma_m=1.5$, $\Delta_{SF}/\gamma_m=8.5$, $g=2\pi \times 0.5 \text{ MHz}$, 1.0 , $\Delta m/\gamma_m=1.5$, (5c) $\Delta/\gamma_m=1.5$, $\Delta_{SF}/\gamma_m=8.5$, $g=2\pi \times 1.5 \text{ MHz}$, 1.0 , $\Delta m/\gamma_m=2.0$,(5d-5f): $g_{ma}=0$, $F=0.05 \text{ N/m}$, $\gamma_m=0.2 \text{ GHz}$, $\Omega=2\pi \times 1 \text{ GHz}$, (5d) $\Delta/\gamma_m=1.0$, $\Delta_{SF}/\gamma_m=8.5$, $g=2\pi \times 0.1 \text{ MHz}$, 1.0 , $\Delta m/\gamma_m=1.0$, (5e) $\Delta/\gamma_m=1.5$, $\Delta_{SF}/\gamma_m=8.5$, $g=2\pi \times 0.5 \text{ MHz}$, 1.0 , $\Delta m/\gamma_m=1.5$, (5f) $\Delta/\gamma_m=1.5$, $\Delta_{SF}/\gamma_m=8.5$, $g=2\pi \times 1.5 \text{ MHz}$, 1.0 , $\Delta m/\gamma_m=2.0$]

Energy is transferred from the strong pump field to the signal mode in connection with the nonlinear interaction term. In our Hamiltonian, the term g open paren b a. to the, $\dagger 2$ end superscript plus b to the \dagger , a. squared, close paren gives the down conversion (Pump goes to two a. photons) and upconversion (wo a. photons goes to Pump). So, to squeeze

the quadrature noise and amplify variances equals numerator, a. plus a. troot of $2 = \frac{a+a^\dagger}{\sqrt{2}}$, $P = \frac{a-a^\dagger}{i\sqrt{2}}$. In this regime, we analyze how much the frequency sponse of the

system (the applied input signals are various frequency regimes) is amplified [48]. We solve it by using the linearised Heisenberg-Langevin equation (numerically using time-evolving operators). In figures 6a –6d, we plot the growth of

less than a.a.plot growth of $\langle aa^\dagger \rangle$ under coherent input for the study of the parametric amplification [49].

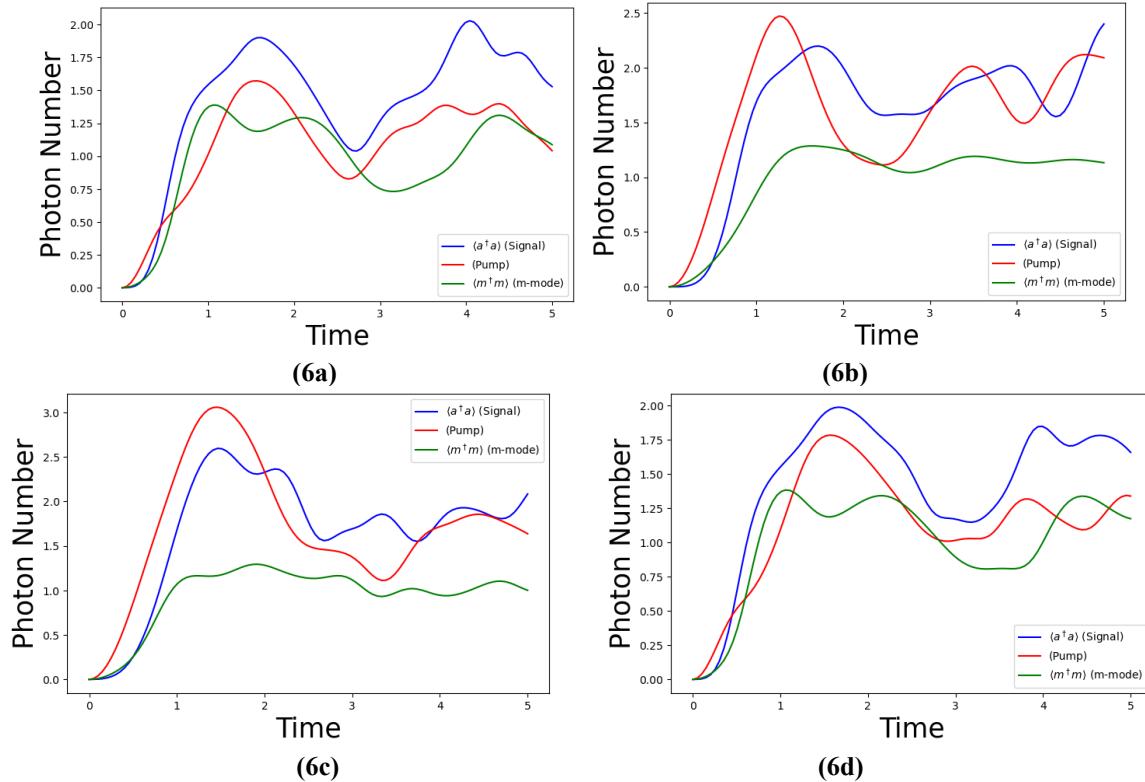


[Fig.6: Represents the Parametric Amplification as a Function of Time. The Different System Parameters Are: $g=2\pi \times 0.1$ MHz, $gma=2\pi \times 1.0$ MHz, $F=0.01$ N/m, $\gamma m=0.2$ GHz, $\Omega=2\pi \times 1$ GHz, (6a) $\Delta/\gamma m=1.0$, $\Delta SF/\gamma m=8.5$, $\Delta m/\gamma m=1.0$, (6b) $\Delta/\gamma m=1.5$, $\Delta SF/\gamma m=8.5$, $\Delta m/\gamma m=2.0$, (6c) $\Delta/\gamma m=1.5$, $\Delta SF/\gamma m=8.5$, $\Delta m/\gamma m=1.0$, (6d) $\Delta/\gamma m=1.5$, $\Delta SF/\gamma m=5.0$, $\Delta m/\gamma m=3.0$]

V. CONCLUSIONS

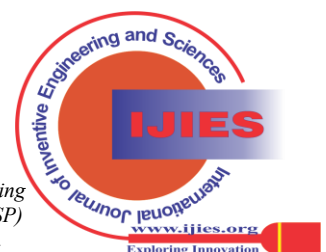
In conclusion, we have investigated the unconventional magnon blockade effect in a cavity magnonic system rotating under a fixed angular speed, the light circulating in the cavity resonator experiences a Sagnac-Fizeau shift, and the cavity resonance frequency is modified by $\omega_k \omega_k + \Delta_{SF_k}$. In this study, we also represent the logarithmic second-order correlation function analytically and numerically. By performing analytical and numerical analyses while tuning different system parameters, we achieved an unconventional magnon blockade effect and a non-reciprocal magnon blockade effect at a fixed angular speed, subscript base, subscript base, omega, end base, sub r. We plot the logarithmic second-order correlation as a function of magnon detuning and Sagnac Fizeau shift, as a function of environmental temperature, and as a function of cavity detuning and magnon detuning. We represent parametric amplification to squeeze quadrature noise and amplify the signal in communication technology. We established the condition of a non-reciprocal coupling regime under controlled temperature and thermal magnon noise. When two photons drive it, complete quantum destructive interference appears and disappears in different paths for two magnon excitations due to the opposite Sagnac Fizeau shifts induced by Fizeau drag, which represents the nonreciprocal unconventional magnon blockade. Our proposal explores the

potential application of quantum communication technology, utilising it to generate a single magnon source and amplify the input signal through parametric amplification factors.

DECLARATION STATEMENT

After aggregating input from all authors, I must verify the accuracy of the following information as the article's author.

- **Conflicts of Interest/ Competing Interests:** Based on my understanding, this article has no conflicts of interest.
- **Funding Support:** This article has not been funded by any organizations or agencies. This independence ensures that the research is conducted with objectivity and without any external influence.
- **Ethical Approval and Consent to Participate:** The content of this article does not necessitate ethical approval or consent to participate with supporting documentation.
- **Data Access Statement and Material Availability:** The adequate resources of this article are publicly accessible.
- **Authors Contributions:** All authors discussed the whole work, read it very carefully, and verified the output profile. AS performed theoretical and numerical calculations, checked graphical outputs, and wrote the paper. PCJ reviewed the paper and analysed the data.



REFERENCES

1. Lasher. G. J. (1964). Analysis of a proposed bistable injection laser. *Solid state Electronics* 7, 707. DOI: <https://doi.org/10.1049/ip-j.1986.0047>
2. Dorsel, A. et al. (1983). Optical bistability and mirror confinement induced by radiation pressure. *Phys. Rev. Lett.* 51, 1550. DOI: <https://doi.org/10.1103/PhysRevLett.51.1550>
3. Yuan. G. et al. (2008). Theoretical and experimental studies on bistability in semiconductor ring lasers with two optical injections. *IEEE J. S. T. Quant. Ele.* 14, 3. DOI: <https://doi.org/10.1109/JSTQE.2008.918058>
4. Jiang. C. et al. (2013). Controllable optical bistability based on photons and phonons in a two-mode optomechanical system. *Phys. Rev.. A* 88, 055801. DOI: <http://doi.org/10.1088/1612-202X/acf046>
5. Li. S. et al. (2017). Optical bistability via an external control field in an all-fibre ring cavity. *Sci. Rep.* 7, 8992. DOI: <https://doi.org/10.1016/j.optlastec.2017.07.052>
6. Yu. C. Sun. L. Zhang. H. and Chen. F. (2018). Controllable optical bistability in a double quantum dot molecule. *IET Optoelectronics* 12, 215. DOI: <https://doi.org/10.1049/iet-opt.2018.0033>
7. Minh. P. L. T. et al. (2018). Optical bistability in a controllable giant self-Kerr nonlinear gaseous medium, electromagnetically induced transparency, and Doppler broadening. *Int. j. opt.*, article id 7260960. DOI: <http://dx.doi.org/10.1155/2018/7260960>
8. Jiang. C. Bian. X. Cui. Y. and Chen. G. (2016). Optical bistability and dynamics in an optomechanical system with a two-level atom. *J. Opt. Am. B* 33, 10. DOI: <https://doi.org/10.1364/JOSAB.33.002099>
9. Li. J. Yu. R. Ding. C. and Wu. Y. (2014). Optical bistability and four-wave mixing with a single nitrogen-vacancy centre coupled to a photonic crystal nanocavity in the weak-coupling regime. *Opt. Express* 22, 15024. DOI: <https://doi.org/10.1364/OE.22.015024>
10. Jiang. L. et al. (2017). Optical bistability and four-wave mixing in a hybrid optomechanical system. *Phys. Lett. A* 381, 3289. DOI: <https://doi.org/10.1016/j.physleta.2017.08.045>
11. Chen. H. J. et al. (2019). Controllable optical bistability and four-wave mixing in a photonic molecule optomechanics. *Nanoscale research letters* 14, 73. DOI: <https://doi.org/10.1186/s11671-019-2893-2>
12. Baas, A. Karr. J. P. Eleuch. H. and Giacobino. E. (2004). Optical bistability in semiconductor microcavities. *Phys. Rev.. A* 69, 023809. DOI: <https://doi.org/10.1103/PhysRevA.69.023809>
13. Kyriienko. O. Liew. T. C. H. and Shelykh. I. A. (2013). Optomechanics with cavity polaritons: Dissipative coupling and unconventional bistability. *arxiv: 1308.2131v1 [cond-mat.mes-hall]*. DOI: <https://doi.org/10.1103/PhysRevLett.112.076402>
14. Zhang. G. Q. Wang. Y. P. You. J. Q. (2019). Theory of the magnon Kerr effect in cavity magnonics. *arxiv: 1903.03754v1 [quant-ph]*. DOI: <https://doi.org/10.1103/PhysRevB.94.224410>
15. Wang. Y. P. et al. (2018). Bistability of cavity magnon polariton. *arxiv: 1707.06509v2[quant-ph]* DOI: <https://doi.org/10.1103/PhysRevLett.120.057202>
16. Kong. C. Xiong. H. and Wu. Y. (2019). Magnon-induced nonreciprocity based on the Magnon Kerr effect. *Phys. Rev.. App.* 12, 034001. DOI: <https://doi.org/10.1103/PhysRevApplied.12.034001>
17. Elliott. M. and Giinossar. E. (2016). Applications of the Fokker-Planck equation in circuit quantum electrodynamics. *arxiv: 1606.08508v1 [quant-ph]*. DOI: <https://doi.org/10.1103/PhysRevA.94.043840>
18. Mukherjee. K. and Jana. P. C. (2019). Optical bistability in a coupled cavity system. *Proceedings of the international conference on optics and electro-optics (ICOL-2019)*. Springer Proceedings in Physics 258, 247. DOI: https://doi.org/10.1007/978-981-15-9259-1_56
19. Gippius. N. A. et al. (2004). Nonlinear dynamics of polariton scattering in semiconductor microcavity: Bistability vs. stimulated scattering. *Eur. Phys. Lett.* 67, 997. DOI: <http://doi.org/10.1209/epl/i2004-10133-6>
20. Larionova. Y. Stolz. W. and Weiss. C. O. (2008). Optical bistability and spatial resonator solitons based on exciton-polariton nonlinearity. *Opt. Lett.* 33, 32.1. DOI: <https://doi.org/10.1364/OL.33.000321>
21. Y. Zhang et al, The multistability in the coupled semiconductor microcavities. *Int. J. Quant. Inf.* 13, 1550053. (2015). DOI: <https://doi.org/10.1142/S0219749915500537>
22. Jing. H. et al. (2018). Nanoparticle sensing with a spinning resonator. *Optica* 5, 1424. DOI: <https://doi.org/10.1364/OPTICA.5.001424>
23. Mirza. I. M. Ge. W. and Jing. H. (2019). Optical nonreciprocity and slow light in coupled spinning optomechanical resonators. *Opt. Exp.* 27, 25515. DOI: <https://doi.org/10.1364/oe.27.025515>
24. Gibbs. H. (1985). *Optical Bistability: Controlling light with light.* (Academic, New York). DOI: https://doi.org/10.1007/978-3-540-38950-7_46
25. Peyghambarian. N. and Gibbs. H. M. (1985). Optical bistability for optical signal processing and computing. *Optical Engineering* 24, 68. DOI: <https://doi.org/10.1117/12.7973427>
26. Xu. L. and Wang. B.C. (2002). Optical spectral bistability in a semiconductor fibre ring laser through gain saturation in an SOA. *IEEE Photon. Tech. Lett.* 14, 149. DOI: <https://doi.org/10.1109/68.980477>
27. Mao. Q. and Lit. J.W. (2003). L-band fibre laser with wide tuning range based on dual-wavelength optical bistability in linear overlapping grating cavities. *IEEE J. Quant. Electron* 39, 1252. DOI: <https://doi.org/10.1002/mop.11198>
28. Faraon, A. et al. (2011). Integrated quantum optical networks based on quantum dots and photonic crystals. *New J. Phys.* 13, 055025. DOI: <http://doi.org/10.1088/1367-2630/13/5/055025>
29. Sete. E.A. and Eleuch. H. (2012). Controllable nonlinear effects in an optomechanical resonator containing a quantum well. *Phys. Rev.. A* 85, 043824. DOI: <https://doi.org/10.1103/PhysRevA.85.043824>
30. Gao. M. et al. (2015). Self-sustained oscillation and dynamical multistability of optomechanical systems in the extremely-large-amplitude regime. *Phys. Rev.. A* 91, 013833. DOI: <https://doi.org/10.1103/PhysRevA.91.013833>
31. Yan. D. et al. (2015). Duality and bistability in an optomechanical cavity coupled to a Rydberg superatom. *Phys. Rev.. A* 91, 023813. DOI: <https://doi.org/10.1103/PhysRevA.91.023813>
32. Mukherjee. K. and Jana. P. C. (2019). Controlled optical bistability in parity-time symmetry micro-cavities: Possibility of all-optical switching. *Physica E: Low-dimensional systems and nanostructures* 117, 113780. DOI: <https://doi.org/10.1016/j.physe.2019.113780>
33. Irvine. W. T. M. et al. (2006). Strong coupling between single photons in semiconductor microcavities. *Phys. Rev.. Lett.* 96, 057405. DOI: <https://doi.org/10.1103/PhysRevLett.96.057405>
34. Yang. Z. et al. (2007). Enhanced second-harmonic generation in AlGaAs microring resonators. *Opt. Lett.* 32, 826. DOI: <https://doi.org/10.1364/OL.32.000826>
35. Andreani. L. C. Panzarini. G. and Gerard. J. M. (1999). Strong-coupling regime for quantum boxes in pillar microcavities: Theory. *Phys. Rev.. B* 60, 13276. DOI: <https://doi.org/10.1103/PhysRevB.60.13276>
36. Skauli. T. et al. (2002). Measurement of the nonlinear coefficient orientation-patterned GaAs and demonstration of highly efficient second-harmonic generation. *Opt. Lett.* 27, 628. DOI: <https://doi.org/10.1364/OL.27.000628>
37. Bergfeld. S. Daum. W. (2003). Second-harmonic generation in GaAs: Experiment versus theoretical predictions of $\chi_{xyz}^{(2)}$. *Phys. Rev. Lett.* 90, 036801. DOI: <http://doi.org/10.1103/PhysRevLett.90.036801>
38. Chen. J. Levine. Z. H. and Wilkins. J. W. (1995). Calculated second-harmonic susceptibilities of BN, AlN, and GaN. *Appl. Phys. Lett.* 66, 9. DOI: <https://doi.org/10.1063/1.113835>
39. Sanford. N. A. et al. (2005). Measurement of second-order susceptibilities of GaN and AlGaIn. *J. App. Phys.* 97, 053512. <https://doi.org/10.1063/1.1852695>
40. Roland. I. et al. (2016). Phase-matched second harmonic generation with on-chip GaN-on-Si microdisks. *Sci. Rep.* 6, 34191. DOI: <https://doi.org/10.1038/srep34191>
41. May. S. et al. (2019). Second-harmonic generation in AlGaAs-on-insulator waveguides. *Opt. Lett.* 44, 1339. DOI: <https://doi.org/10.1364/OL.44.001339>
42. GMalykin. B. (2000). The Sagnac effect: correct and incorrect explanations. *Phys. Usp.* 43, 1229. DOI: <https://doi.org/10.1070/pu2000v043n12ABEH000830>
43. Franke, A. S. Gibson, G. Boyd, R. W. Padgett. M. J. (2011). Rotary photon drag enhanced by a slow-light medium. *Science* 333, 65. DOI: <https://doi.org/10.1126/science.1203984>
44. Maayani. S. et al. (2018). Flying couplers above spinning resonators generate irreversible refraction. *Nature* 558, 569. DOI: <https://doi.org/10.1038/s41586-018-0245-5>
45. Arita. Y. Mazilu. M. and Dholakia. K. (2013). Laser-induced rotation and cooling of a trapped microgyroscope in a vacuum. *Nat. Comm.* 4, 2374. DOI: <https://doi.org/10.1038/ncomms3374>
46. Monteiro. F. Ghosh. S. Assendelft. E. C. V. and Moore. D. C. (2018). Optical rotation of levitated spheres in high vacuum. *Phys. Rev. A* 97, 051802(R). DOI: <http://dx.doi.org/10.1103/PhysRevA.97.051802>
47. Ahn. J. et al. (2018). Optically levitated nano-dumbbell torsion balance and GHz nanomechanical rotor. *Phys. Rev. Lett.* 121, 033603.

- DOI: <https://doi.org/10.1103/PhysRevLett.121.033603>
48. Reimann, R. et al. (2018). GHz rotation of an optically trapped nanoparticle in a vacuum. Phys. Rev. Lett. 121, 033602.
DOI: <https://doi.org/10.1103/PhysRevLett.121.033602>
49. Wang, K. Wu, Q. Yu, Y. F. Zhang, Z. M. (2019). Nonreciprocal photon blockade in a two-mode cavity with a second-order nonlinearity. Phys. Rev. A. 100, 053832.
DOI: <https://doi.org/10.1103/PhysRevA.100.053832>

AUTHOR'S PROFILE



Anjan Samanta completed a Master of Science from Vidyasagar University. The author currently works as a research fellow at Vidyasagar University. His research interests include quantum optics, quantum optomechanics, cavity magnonics, and photon blockade.



Pinku Jana completed a Master of Science from Vidyasagar University. The author currently works as a research fellow at Vidyasagar University. His research interests include quantum optics, quantum optomechanics, cavity magnonics, and photon blockade.



Paresh Chandra Jana received his PhD from IIT Kharagpur in 1995 on Normal State transport properties of High-Tc superconducting Oxides. The author is a Former Scientist B in DRDO (Jodhpur Defence Laboratory) and winner of the DRDO Technology Cash Award, and is currently a professor at the Department of Physics, Vidyasagar University. His research interests include conducting polymers, ferroelectrics, quantum optics, and quantum optomechanics. Notable recent publications include Controlled optical bistability in parity-time-symmetric coupled micro-cavities: Possibility of all-optical switching, Physica E: Low-dimensional Systems and Nanostructures, 117: 113780 (2019), Journal of Materials Science: Materials in Electronics, 30 (3): 2154-2165 (2019), Optically induced transparency in coupled micro-cavities: tunable Fano resonance, European Physical Journal D., 73: 264 (2019).

APPENDIX [A]

By using the Python program, we can solve the probability amplitudes.

$$C_{01} = -\frac{FC_{00} + g_{ma}C_{10}}{(\Delta_m + 2(\Delta + \Delta_{SF}))}$$

$$C_{10} = -\frac{\Omega C_{00} + g_{ma}C_{01} + 2gC_{20} + gC_{11}}{(\Delta + \Delta_{SF})}$$

$$C_{20} = \frac{\sqrt{2}\Omega C_{10}}{2(\Delta + \Delta_{SF})}$$

$$C_{02} = \frac{\sqrt{2}F(FC_{00} + g_{ma}C_{10})}{(\Delta_m + 2(\Delta + \Delta_{SF}))^2} - \frac{g_{ma}C_{20}}{2(\Delta_m + 2(\Delta + \Delta_{SF}))}$$

$$C_{11} = -\frac{gC_{01} + g_{ma}C_{20}}{\Delta + \Delta_{SF} + \Delta_m + 2(\Delta + \Delta_{SF})}$$

Disclaimer/Publisher's Note: The statements, opinions and data contained in all publications are solely those of the individual author(s) and contributor(s) and not of the Blue Eyes Intelligence Engineering and Sciences Publication (BEIESP)/ journal and/or the editor(s). The Blue Eyes Intelligence Engineering and Sciences Publication (BEIESP) and/or the editor(s) disclaim responsibility for any injury to people or property resulting from any ideas, methods, instructions or products referred to in the content.